



Article

Short-Term and Long-Term Replenishment of Water Storage Influenced by Lockdown and Policy Measures in Drought-Prone Regions of Central India

Soumendran N. Bhanja ^{1,*} and M. Sekhar ^{1,2}

¹ Interdisciplinary Centre for Water Research, Indian Institute of Science, CV Raman Rd., Bangalore 560012, Karnataka, India; muddu@iisc.ac.in

² Department of Civil Engineering, Indian Institute of Science, CV Raman Rd., Bangalore 560012, Karnataka, India

* Correspondence: bhanjasn@ornl.gov; Tel.: +91-8653717098

Abstract: Central India faces a freshwater shortage due to its diverse terrain, sudden change in precipitation patterns and crystalline rock covered subsurface. Here, we investigate the patterns in terrestrial water storage anomaly (TWSA) over the last two decades, and also study the influence of the COVID-19 lockdown on TWSA in the drought-prone regions of central India, mostly covering the Vidarbha region of the Indian state of Maharashtra. The Vidarbha region is arguably the most drought-affected region in terms of farmer suicides due to crop failure. Our forecast data using multiple statistical approaches show a net TWSA rise in the order of 3.65 to 19.32 km³ in the study area in May 2020. A short-term rise in TWSA in April–May of 2020 is associated with lockdown influenced human activity reduction. A long-term rise in TWSA has been observed in the study region in recent years; the rising TWSA trend is not directly associated with precipitation patterns, rather it may be attributed to the implementation of water management policies.

Keywords: terrestrial water storage anomaly (TWSA); water storage forecasting; prediction; GRACE; GRACE follow-on; central India; Vidarbha



Citation: Bhanja, S.N.; Sekhar, M. Short-Term and Long-Term Replenishment of Water Storage Influenced by Lockdown and Policy Measures in Drought-Prone Regions of Central India. *Remote Sens.* **2022**, *14*, 1768. <https://doi.org/10.3390/rs14081768>

Academic Editors: Jolanta Nastula and Monika Birylo

Received: 28 February 2022

Accepted: 4 April 2022

Published: 7 April 2022

Publisher's Note: MDPI stays neutral with regard to jurisdictional claims in published maps and institutional affiliations.



Copyright: © 2022 by the authors. Licensee MDPI, Basel, Switzerland. This article is an open access article distributed under the terms and conditions of the Creative Commons Attribution (CC BY) license (<https://creativecommons.org/licenses/by/4.0/>).

1. Introduction

Freshwater availability is a crucial issue in central India due to its diverse terrain, changing precipitation patterns and non-favorable subsurface structure mostly composed of jointed or fractured crystalline rocks [1]. Semi-arid climate prevails in this region and a sudden decline in monsoonal precipitation often leads to severe water scarcity and drought [2]. As a result, most of these regions are characterized as drought prone, and management programs are already in place in the form of preventive measures by the government authorities [3]. Hydrological drought is one of the reasons for crop failure as well as farmer distress in central India [4]. The eastern part of the Indian state of Maharashtra, the Vidarbha region, has been subjected to large-scale droughts as well as the largest number of farmer suicides in India over the years [5,6]. Maharashtra (mostly the eastern part) reported a massive 3030 incidents of farmer suicides in 2015 alone, mostly linked to bankruptcy and indebtedness (>42%) as a result of crop failure [7]. Long-term patterns of water storage change need to be urgently investigated in this region to enable proper management of the available water resources.

To contain the extent of the COVID-19 pandemic, India undertook a nation-wide lockdown for 68 days between 24 March and 31 May 2020 (https://en.wikipedia.org/wiki/COVID-19_pandemic_lockdown_in_India#Lockdown accessed on 29 July 2020). COVID-19 spreads havoc in densely populated countries like India, with 513,226 deaths and ~42.89 million total infections up to 25 February 2022 [8]. Maharashtra has been the worst affected state in India, with >18% of the total infections and ~28% of the total deaths

reported up to 26 February 2022 [9]. As a result, most economic activities in Maharashtra, including agriculture, have stalled for a prolonged period within the state, particularly during the nationwide lockdown in 2020. This led to a unique test bed to study the human influences on the hydrologic cycle.

Water storage prediction/forecasting has been performed over the years using a suite of classical and contemporary statistical methods. Regression-based analyses are performed to estimate groundwater level responses from long ago [10–12]. Apart from linear regression estimates, auto regressive (AR), moving average (MA) and a combination of these two, such as the auto regressive moving average (ARMA) and auto regressive integrated moving average (ARIMA) have been widely used in hydrology over the years [13]. With the advent of intensive computing resources, artificial intelligence (AI) based approaches have been widely applied in hydrologic modeling. Artificial neural network (ANN) based approaches have also been used for a long time in both stream flow [14] and groundwater level predictions [15]. Many other AI based approaches are available nowadays, and are providing encouraging outputs in parts of the globe with less computational requirement [13,16–18].

We used terrestrial water storage (TWS) data from the Gravity Recovery and Climate Experiment (GRACE) and its Follow-on (GRACE-FO) missions between April 2002 and August 2020. Both of the GRACE missions are designed to monitor the continuous temporal variability in Earth’s gravity field that may arise as a result of the mass changes in atmospheric, oceanic, and terrestrial water and solid earth domains across the globe [19–21]. TWS changes are estimated after eliminating the influences of solid earth processes [22] and the atmospheric and oceanic processes [23]. Here, TWS anomalies are investigated in the Vidarbha region (Figure 1) to estimate the influence of either the COVID-19 linked lockdown or other factors on the local water budget. We also study the long-term patterns of TWS and their controlling factors in the drought prone region. With the help of multiple statistical approaches, we have attempted to quantify the net change in TWSA due to the influence of lockdown and stalled human activities.

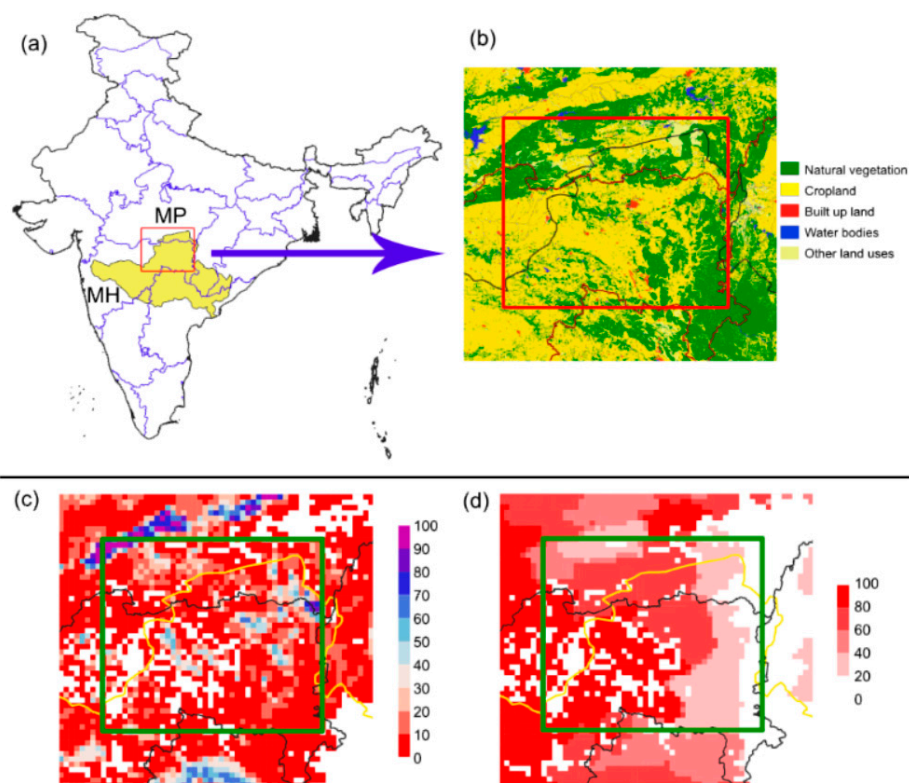


Figure 1. (a) The study region is marked by the red line. Administrative boundaries of Indian states (MH: Maharashtra; MP: Madhya Pradesh) and the Godavari river basin are shown. (b) Land use land

cover data for 2005 are plotted using data from the Oak Ridge National Laboratory's database [24]. (c) The irrigation equipped area as a percentage of total land area and (d) the percentage of area irrigated by groundwater out of the total irrigation equipped area (plotted using data from Siebert et al. [25]).

2. Data and Methods

2.1. Study Area

Study area (Figure 1a, red box) includes the Vidarbha region in Maharashtra and parts of southern Madhya Pradesh. Study area covers parts of 11 districts of Maharashtra (Akola, Amravati, Bhandara, Chandrapur, Garhchiroli, Gondiya, Hingoli, Nagpur, Wardha, Washim, Yavatmal) and five districts of Madhya Pradesh (Balaghat, Betul, Chhindwara, Harda, Seoni). The subsurface is mostly composed of basalt with some patches of quartzite, schist and granite observed [26]. Black soil dominates the soil types in the area with its occurrence in the weathered zone that sometimes reach up to 20 m [27]. The region receives annual precipitation in the range of 600–1200 mm with low to high values in a western to eastern direction [28]. More than 90% of the precipitation occurs in the June to September monsoon months (Figure 2a). The study area constitutes a $\sim 3^\circ \times 3^\circ$ mascon block (mass concentration blocks that optimally represent GRACE's inter-satellite ranging observations) in GRACE JPL's mascon solution [29]. The recent GRACE-based terrestrial water storage (TWS) products are released at the spatial resolution of a $0.5^\circ \times 0.5^\circ$ grid, however, their native resolution is $\sim 3^\circ \times 3^\circ$, and one of the native pixels selected here [29–31]. Natural vegetation and cropland covers more than 90% of the study area (Figure 1b). Eastern and northern parts are mostly covered by natural vegetation while the south-western part is dominated by cropland. Areas equipped for irrigation show a coverage of 10–80%, while most of the areas are within a 30% irrigation equipment coverage area in 2013 (Figure 1c). Groundwater supports the majority of the irrigation demand in the south-western part in which croplands are mostly found and the precipitation rate is comparatively lower; surface water irrigation is dominant in the eastern part (Figure 1d). More than 50% of the irrigated land was supported by groundwater in Vidarbha [32]. The absence of major rivers and streams in this region further increases groundwater dependency in non-monsoon months.

2.2. GRACE TWSA

Gridded ($0.5^\circ \times 0.5^\circ$) RL06 TWS mascon solution change data are obtained from the National Aeronautics and Space Administration (NASA) Jet Propulsion Laboratory (JPL) archive [29–31]. Satellite laser ranging data are used for estimating the degree 2 and order 0 coefficients [33]. The influence of elastic deformation of the subsurface due to the post glacial rebound signals are modeled following A et al. [34]. Post processing filters are not used for noise removal, rather a priori information is used [29]. In this approach, $3^\circ \times 3^\circ$ mass concentration blocks cover the entire globe, and the dimensions serve as the native resolution of the data product [29]. The coastline resolution improvement (CRI) filter was used in the processed data to remove the ocean signal [29]. To increase the resolution of the data and derive the output at $0.5^\circ \times 0.5^\circ$ globally, a Community Land Model (CLM) hydrology run was performed at the same resolution to determine the scale/gain factors [30]. As recommended by the data providers, we used scale factors to improve the TWS estimates at each pixel data. We obtained the data for 186 months between April-2002 and May-2020. TWS anomalies are computed after removing the long-term mean TWS from the individual temporal data points at the pixel level ($0.5^\circ \times 0.5^\circ$).

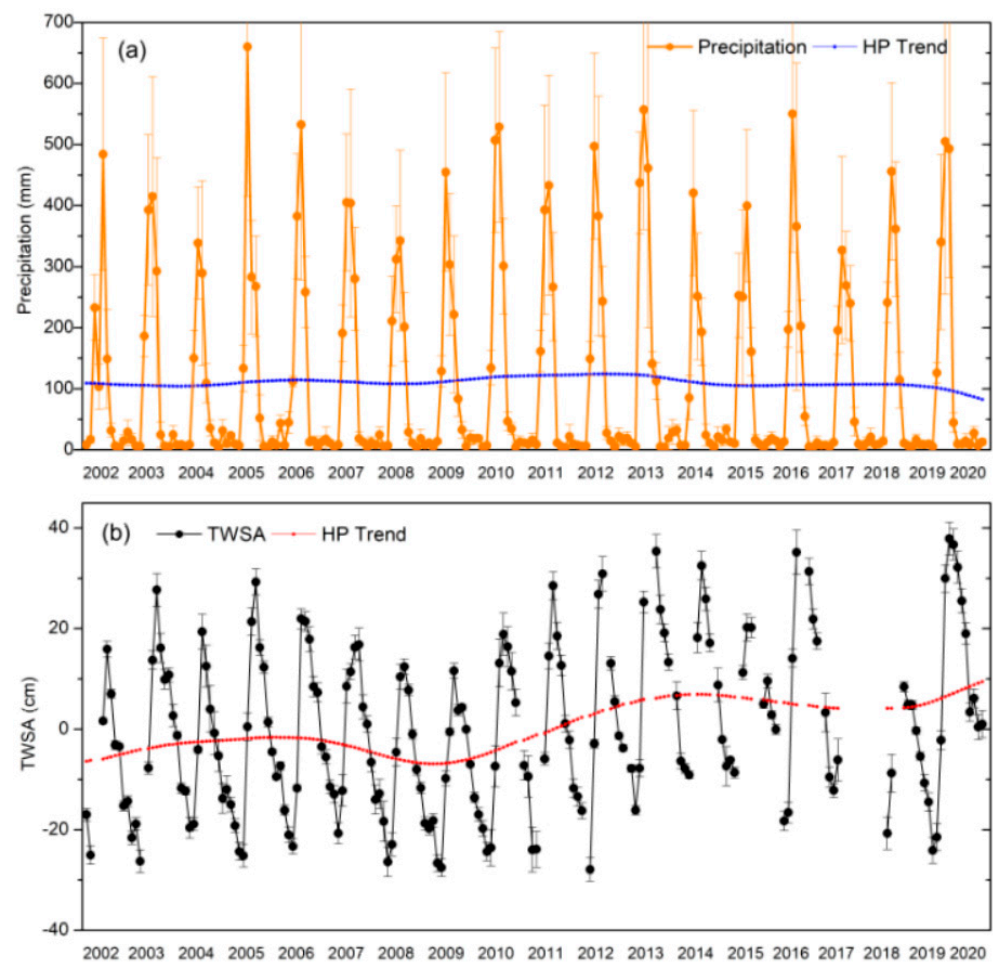


Figure 2. (a) Monthly mean precipitation time-series. Hodrick–Prescott (HP) trend is shown in blue color. (b) Monthly mean terrestrial water storage (TWS) anomaly and its HP trend in the study region.

2.3. Precipitation and Evapotranspiration

We used the $0.05^\circ \times 0.05^\circ$ gridded rainfall data from the Climate Hazards group Infrared Precipitation with Stations (CHIRPS) archive produced by the United States Geological Survey (USGS) and the Climate Hazard Center of the University of California Santa Barbara [35]. Both the gauge-based precipitation estimates as well as the infrared-based cold cloud duration estimates from the satellite observations are blended together to create the data [35]. Some of the major advantages of CHIRPS are its very low latency period (less than a month) and the high spatial resolution ($0.05^\circ \times 0.05^\circ$) [35]. Precipitation data from CHIRPS are well comparable with the gauge-based estimates in India [36] and on the high mountain Asia region [37].

We used evapotranspiration (ET) estimates from the Global Land Data Assimilation System (GLDAS) model simulations [38]. ET estimates from two separate land surface models, i.e., Noah and Catchment Land Surface Model (CLSM) are used. CLSM L4 data (v. 2.10) and Noah L4 data (v. 2.10) are used. ET estimates from the Noah model are reported to perform better in Tibetan plateau [39] and in parts of the United States [40]. Apart from Noah ET estimates, recent studies show CLSM ET estimates are also performing well in parts of the United States [41].

2.4. Forecasting Techniques

In order to show the influence of the lockdown-linked human activity reduction on TWSA, we performed several statistical tests to forecast the TWSA for the last 7 months from November 2019 to May 2020. The study period was restricted to May-2020 as the

monsoon starts in June and significantly influence the water availability. Precipitation data from 2002 to 2020 indicates only 6.43% of the total annual rainfall has occurred during the 7-month time period, i.e., November to May (Figure 2). With precipitation being the major driver of TWSA, and assuming irrigation patterns have not changed over the years, we have performed univariate analyses using the TWSA data between August 2002 and October 2019 (207 months) as an input. Missing GRACE TWSA data are filled by linear interpolation.

The following six approaches are used for forecasting the TWSA. First, we performed regression analyses on the time-series data to forecast the TWSA data. Autoregressive integrated moving average (ARIMA) is one of the most widely used approaches for time series forecasting since its inception in the 1970s [10,42–44]. ARIMA models compute the autocorrelation in the data. The ARIMA model can be represented as [10,42,44]:

$$\left(1 - \phi_1 B - \dots - \phi_l B^l\right) (1 - B)^m y_t = c + (1 + \theta_1 B + \dots + \theta_n B^n) \quad (1)$$

where the first part represents the autoregressive (AR) functions of the backshift operator (B). The second part represents the functions of differences, and the last part represents the moving average (MA) functions. l , m and n represent the order of the AR part, the degree of the first differencing and the order of the MA part, respectively. c is a random component.

Exponential smoothing (ETS) is another widely used approach for time series forecasting originally introduced by Brown and Holts in the 1960s [45–48]. ETS is a state space model that can simulate the level, trend and seasonal data change over time [49]. Please see Gardner [48,49] and Hyndman et al. [44] for more details on the functions of different types of ETS models.

A feed forward neural network with a single hidden layer is applied through the neural network autoregression (NNAR) model. Here, time lagged TWSA values are used as an input in the model to compute the forecast output.

Seasonal and trend decomposition through the Loess smoother (STL) method was applied on the data following Cleveland et al. [50]. In this process, the time-series data (Y_t) has been disaggregated into trend (T_t), seasonal (S_t) and remainder (R_t) components:

$$Y_t = T_t + S_t + R_t \quad (2)$$

We use another state space model named TBATS (T for Trigonometric regressors to model multiple-seasonalities; B for Box-Cox transformations; A for ARMA errors; T for trend; S for seasonality) to perform the TWSA forecast. In a completely automated manner, TBATS employs Fourier equations with an exponential smoothing state space model along with a Box-Cox transformation [51]. The newly developed method was introduced for the complex seasonal data. Please see De Livera et al. [51] for more details on this method.

2.5. Forecasting Performance Indicators

The performance of the forecast data is examined using statistical approaches, comparing with the observed TWSA. Nash–Sutcliffe efficiency (NSE), percent bias (PBIAS), and root mean square error to standard deviation ratio (RSR) have been widely used in hydrology over the years to test the performance of the predictors [52]. NSE can be represented as the ratio of residual variance and data variance [53].

$$\text{NSE} = 1 - \left[\frac{\sum_{i=1}^n (x_i - y_i)^2}{\sum_{i=1}^n (x_i - \bar{x})^2} \right] \quad (3)$$

where, x_i and y_i represent the observed and simulated values; i ($= 1, 2, 3, \dots, n$) indicate the number of data points; \bar{x} and \bar{y} representing the mean values.

The average deviation of the forecast TWSA from the observed values is represented as PBIAS [54]).

$$\text{PBIAS} = \frac{\sum_{i=1}^n (x_i - y_i) \times 100}{\sum_{i=1}^n x_i} \quad (4)$$

$$\text{RSR} = \frac{\sqrt{\sum_{i=1}^n (x_i - y_i)^2}}{\sqrt{\sum_{i=1}^n (x_i - \bar{x})^2}} \quad (5)$$

The root mean square error (RMSE), mean absolute error (MAE) and the Pearson's correlation coefficient (R) are also computed to show the deviation of forecast TWSA from the observed values [55].

$$\text{RMSE} = \sqrt{\frac{\sum_{i=1}^n (x_i - y_i)^2}{n}} \quad (6)$$

$$\text{MAE} = \frac{\sum_{i=1}^n |x_i - y_i|}{n} \quad (7)$$

$$\text{Pearson's correlation (R)} = \frac{\sum_{i=1}^n (x_i - \bar{x})(y_i - \bar{y})}{\sqrt{\sum_{i=1}^n (x_i - \bar{x})^2} \sqrt{\sum_{i=1}^n (y_i - \bar{y})^2}} \quad (8)$$

3. Results

3.1. Precipitation and TWSA Patterns

Precipitation shows a strong seasonality with the highest recorded values in July and August (Figure 2a). Hodrick–Prescott (HP) trends are computed to separate the long-term trend of precipitation from the intra-annual cycle components [56,57]. The HP trend in precipitation shows a decreasing pattern in recent years. On the other hand, TWSA shows an increasing HP trend in recent years. TWSA signals exhibit strong seasonal variability with highest values from August to November (Figure 3). The intra-annual rise in TWSA during pre-monsoon to monsoon months is linked to precipitation patterns, however, the long-term HP trend in TWSA is not explainable by precipitation only.

Cross-correlation analysis between monthly precipitation and TWSA data shows the best correlation results for 2-month lagged precipitation ($r = 0.68$, $p < 0.001$) followed by 1-month lagged precipitation ($r = 0.65$, $p < 0.001$). Precipitation influence on TWSA thus would be better observed in a 1-2 month lag time period. January to May monthly mean TWSA values between 2002 and 2020 show the highest monthly TWSA values in 2020 in all of the 5 months. The precipitation rate was found to be the third highest during 2019–2020 in 2002–2020 (Figure S1).

Annual TWSA data show strong seasonality, with the highest values during the monsoon months (Figure 3). This is an obvious fact in the study area, as precipitation is the major in-flow component of the hydrological cycle. The lowest TWSA values are found in the pre-monsoon months of May and June. The highest TWSA values in April and May are observed in 2020. Interestingly, TWSA in April and May 2020 show positive TWSA when comparing all time values that might result from the restricted human activities in the lockdown period, including irrigation (Figure 4). Although it is difficult to quantitatively distinguish the influence of 2019–2020 precipitation and the reduced human activities during lockdown on TWSA, the occurrence of positive TWSA during the pre-monsoon (April–May) period definitely show a ray of hope in this drought-prone region.

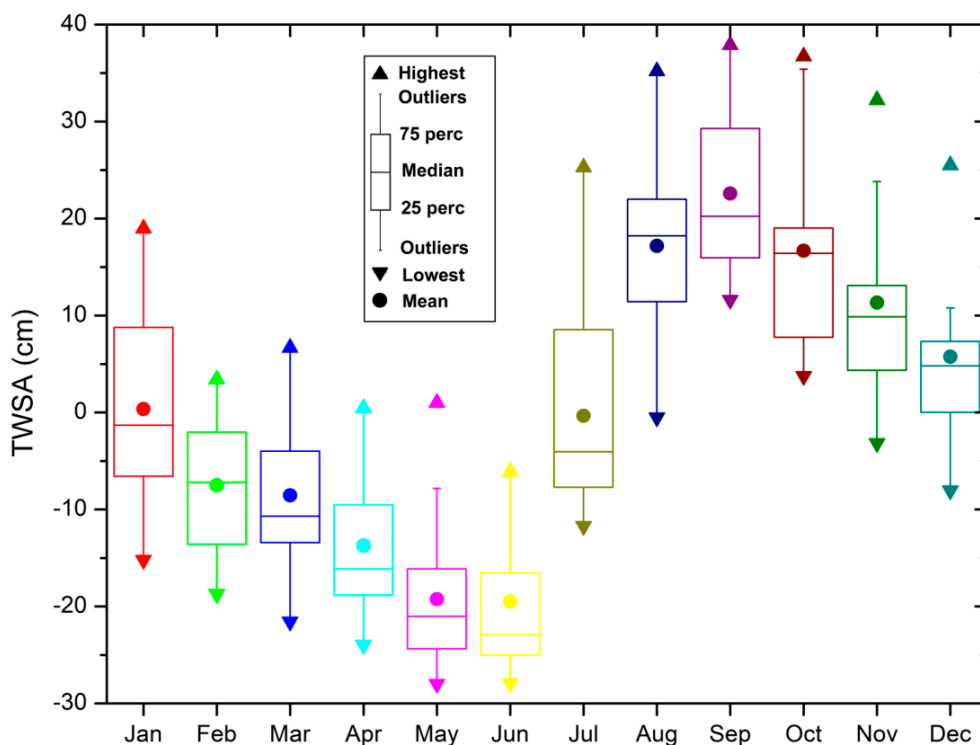


Figure 3. Monthly TWSA data distribution during August 2002 and May 2020.

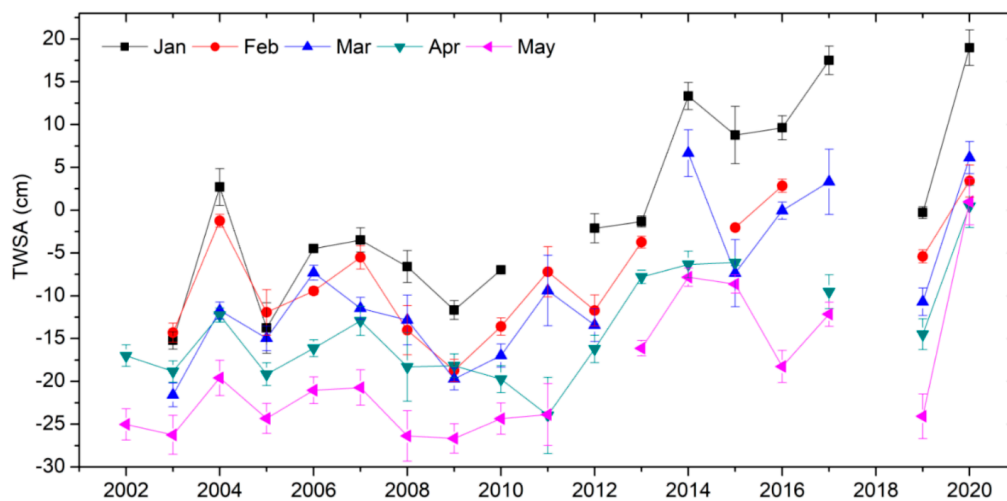


Figure 4. Monthly mean TWSA in January to May during 2002–2020.

Quarterly, in situ groundwater level data from the Central Groundwater Board (CGWB) in this region show a general long-term increase during 2003–2017 (Figure 5). We selected the wells with continuous data records in the study period and have at least three out of four observations per year. The data show an increasing groundwater level trend in 233 out of 347 observation wells (Figure 5a). Mean quarterly groundwater levels show increasing values (Figure 5b) at rates of 3.31 cm/yr.

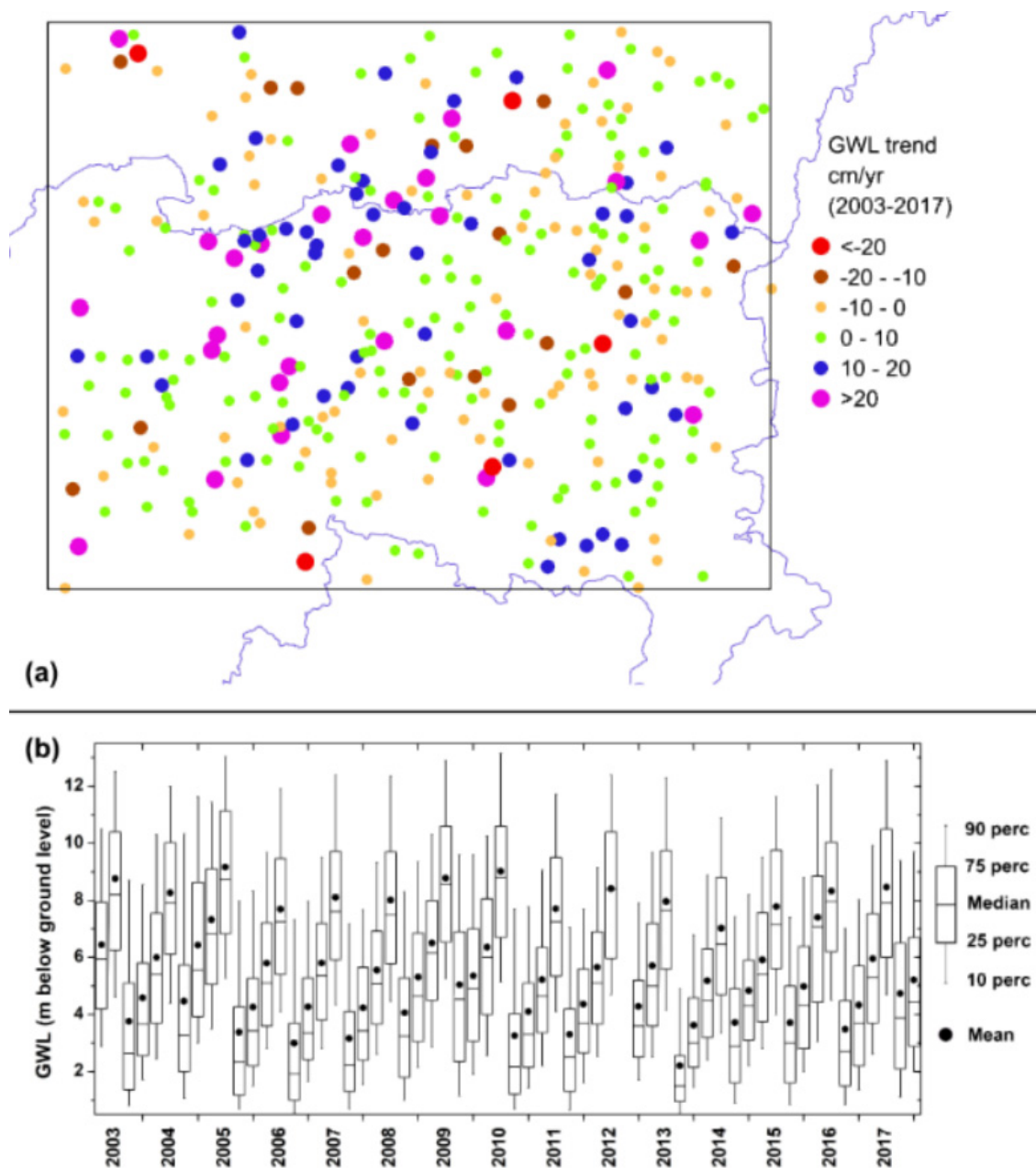


Figure 5. (a) Spatial trends in in situ groundwater level between 2003 and 2017; (b) box plot of in situ groundwater level ($n = 347$). Symbols representing the mean, median, maximum, 10th percentile, 25th percentile, 75th percentile and 90th percentile are shown in inset.

3.2. Evapotranspiration and TWSA Patterns

ET provides cumulative information on seasonal surface water (river, lakes, tanks, ponds, dams, etc.) availability and irrigation if temperature is not varying (for example, on comparing a particular seasonal data for multiple years) and the transpired fraction by the incident plant species. ET also exhibits strong seasonality (Figure 6a) and mostly follow precipitation patterns ($r > 0.62$, $p < 0.001$; with 1-month lag, $r = 0.81$, $p < 0.001$). Both CLSM and Noah-based ET values are well correlated with the TWSA ($r > 0.66$, $p < 0.001$). Distribution of monthly ET values between January and May of 2002–2020, along with the 2020 values, are shown in Figure 6b. ET values from both of the models are observed to be at the highest in January and February 2020 as the irrigation intensity increases in recent years, however, they are a little lower than the highest monthly ET values in March

to May-2020 (Figure 6b). Comparatively higher freshwater availability in March, 2020, is observed through TWSA estimates supporting the higher surface water availability. On the other hand, without any significant change in precipitation in April and May, 2020, from its long-term mean, a sudden decrease in ET from January to March 2020 values might indicate a reduction in irrigation imposed by the lockdown (Figure 6c,d).

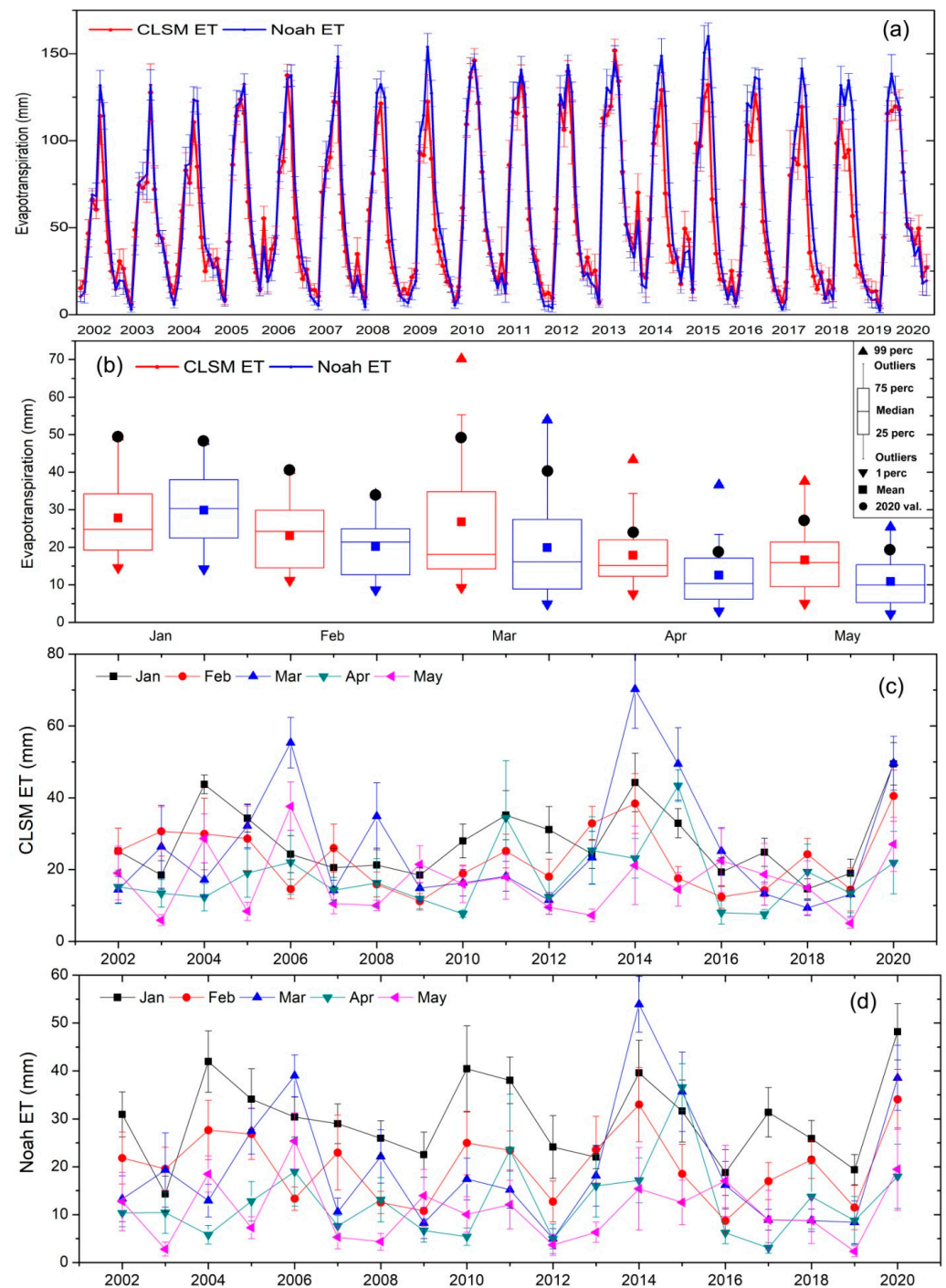


Figure 6. (a) Monthly mean evapotranspiration (ET) from the two land surface models, CLSM and Noah simulation in 2002–2020. (b) Box plot of monthly ET data between January and May. Box, whisker and symbols represent the statistics shown in the inset. Monthly values of (c) CLSM ET and (d) Noah ET.

3.3. Statistical Forecasting of TWSA

In order to investigate the TWSA rise in April–May 2020, we have performed multiple statistical forecasting analyses using the data up to October 2019 as input, and predicted the TWSA for the next 7 months, i.e., November 2019 to May 2020 (Figure 7). The 95% confidence interval for different approaches has shown the uncertainties associated with the forecasting experiment. Performance statistics show the best forecast data from the ETS method followed by the STL method (Table 1; Figure 7). Both of the forecast values overestimated the TWSA data in February to April 2020, with underestimation in May 2020 (Figure 7). The forecast TWSA values from other methods largely underestimate the observed TWSA in May 2020 (Figure 7). As already discussed, it is very difficult to separate out the influence of the pandemic-linked lockdown on TWSA rise, considering the multiple feedbacks associated with the components of hydrological cycle. Our forecast values considering purely stochastic approaches provide some information on the quantitative rise in TWSA values considering a business as usual scenario. Our analyses indicate an overall TWSA rise of 3.65 to 19.32 km³ (estimated based on May 2020 values only), which is most likely linked with COVID-19 lockdown in the study area.

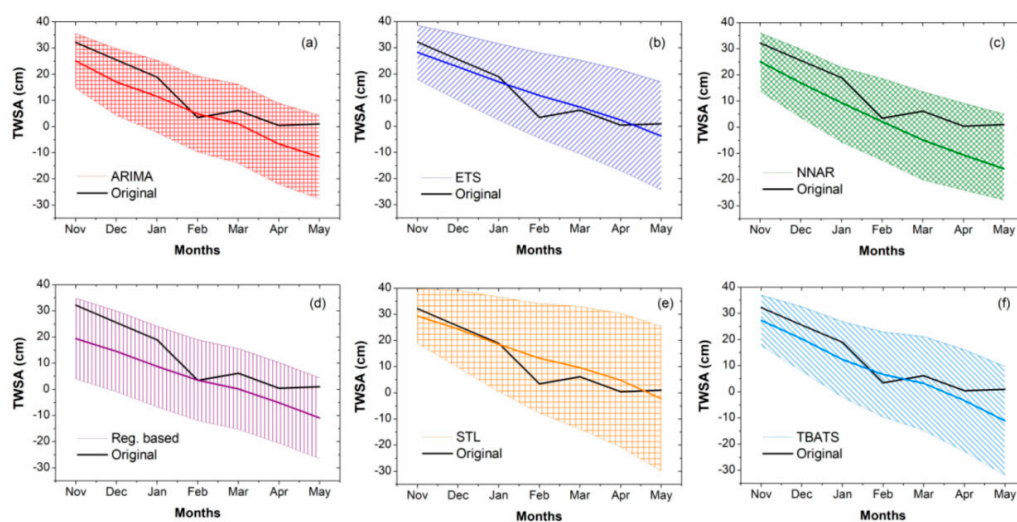


Figure 7. Comparison of forecast performances between observed (GRACE) and forecast (six stochastic models) TWSA from November 2019 to May 2020. The following stochastic models are used: (a) ARIMA (Autoregressive integrated moving average); (b) ETS (Error, Trend, Seasonal or the Exponential Smoothing); (c) NNAR (Neural Network Autoregression); (d) Reg. based (time-series regression based); (e) STL (Seasonal and trend decomposition through Loess smoother) and (f) TBATS (T for trigonometric regressors to model multiple-seasonalities; B for Box–Cox transformations; A for ARMA errors; T for trend; S for seasonality). 95% confidence interval is shown as patterns.

Table 1. Performance statistics of 6 statistical forecasting methods used for TWSA forecasting.

	ARIMA	ETS	NNAR	Regression Based	STL	TBATS
NSE	0.59	0.87	0.26	0.40	0.85	0.73
PBIAS %	52.66	2.03	74.54	65.28	−11.58	36.75
RSR	0.59	0.33	0.80	0.72	0.36	0.49
RMSE	7.67	4.24	10.30	9.23	4.59	6.27
MAE	7.01	3.57	9.34	8.23	3.60	5.54
R	0.95	0.94	0.95	0.94	0.93	0.94

4. Discussions

4.1. Influence of Policy Change on Long-Term TWSA Patterns

Long-term TWSA and precipitation HP trends are negatively correlated ($r = -0.22$, $p = 0.001$). Water management policy implementation in Maharashtra might have played a crucial role in this rise in TWSA from 2011 onwards. An intensive irrigation project was undertaken by the government agencies to improve the agriculture productivity in the Vidarbha region in 2012 [58]. Two separate schemes, Jalyukt Shivar (JYS), and Galmukt Dharan and Galyukt Shivar (GDGS), were introduced in 2014 as a 5-year program [4]. JYS was planned to utilize the decentralized water to support irrigated cropland. De-silting was done in the water tanks in GDGS, and the silts were used in farmland to support productivity. Both of the plans facilitate groundwater recharge, and approximately 25,000 villages were planned to be made drought-proof through these policy implementations [4]. Prior to these policy changes, another policy change (the Maharashtra Management of Irrigation Systems by Farmers Act) was introduced in 2005 to improve the water management scenario in Maharashtra [59]. Furthermore, the Maharashtra Groundwater Act (1993) was previously introduced to regulate the groundwater abstraction activities in depleted regions [32]. A recent World Bank and Government of India funded project started from 2018 on climate resilient agriculture with one of the primary aims to improve water security at farm level [60]. The ongoing project will continue until 2024 and envisions to contribute to efficient irrigation water usage, construction of surface and subsurface structures, etc. These ongoing sustainable management practices would cause a net reduction in water usage and thus improve the water availability in the area.

A general declining long-term precipitation trend does not explain the long-term rise in TWSA (Figure 2). A rise in groundwater storage has been observed in parts of western and southern India due to policy implementation [28]. Similar reasons (as discussed in the earlier section) may have played a major role in the long-term TWSA rise in this region. Maharashtra leads the way in dam construction in India, with 2354 large dams out of the total 5701 constructed large dams in India [61]. These artificial structures induce groundwater recharge and result in groundwater replenishment in these crystalline rock structures [62]. Even a small-scale artificial recharge structure promotes a groundwater level rise of as much as 2.8 m in nearby dug wells in basaltic terrain [63]. Our observation of a 1–2 month lagged relationship of TWSA with precipitation is consistent with the findings of Frappart et al. [64] in the Amazon basin, and the findings of Prakash et al. [65] in northern India. Both the studies reported limited long-term influence of precipitation on TWSA patterns in their respective study regions.

4.2. Change in Cropping Patterns

We used the MOD13C2 (v006) monthly normalized difference vegetation index (NDVI) data products from the NASA's Moderate Resolution Imaging Spectroradiometer (MODIS) sensors on Terra satellite [66]. Shrubs, grassland and some matured crops exhibit NDVI in the range of 0.2 to 0.5, while dense forest and fully grown crops can exhibit NDVI with values > 0.6 [67]. Bhanja et al. [68] observed a strong relationship between NDVI and groundwater storage in parts of India. We used NDVI data to further investigate the TWSA patterns. Pulses and wheat are the two major varieties of food crops that are grown in the study area during the rabi season. Cotton is one of the major crops grown in this region covered by black soil [58]. Figure 8 shows the NDVI values between January and May in 2016–2020. NDVI values are found to be higher in January and continue reducing until they reach their lowest values in May. On comparing the values in 2016–2020, NDVI values are found to be the highest in 2020. The four districts in Maharashtra (Amravati, Nagpur, Gadchiroli and Chandrapur) that show unusually higher rates (116–264%) of cotton cropping area in 2020 compared to the 2016–2019 average values are marked in red color in Figure 8. High rates of cotton cropping may also increase transpiration, particularly in January and February 2020 as observed in Figure 6. Cotton sowing generally starts in June–July and harvesting/picking extends up to February in the Vidarbha region, and

intercropping with some pulses (pea, gram, sorghum, etc.) is practiced [69]. Cotton exhibits a diverse range of NDVI values from the growing stage (0.19–0.30) to blooming (0.30–0.42), and finally to the picking/harvesting phase (0.34–0.07), with occasional maximum values of 0.65 during the growing and blooming phase [70]. The distinct change in NDVI between February and March might be associated with the harvesting time of cotton and preparation of the land for other crops; this is not clear in 2020 (Figure 8). Similar to cotton, wheat also exhibits dynamic NDVI values during its growth at a range of 0.25 to 0.85 [71]. The cropped areas for other rabi crops including wheat (district-wise cropped area in 2020 comparable to 2016–2019 data) and gram (district-wise cropped area in 2020 comparable to 2016–2019 data with some exceptions) show near normal values in 2020 compared to the 2016–2019 estimates. Normal wheat sowing time in central India extends up to the second week of December [72]. Wheat also requires additional step-wise irrigation, a total of six times for its growth [72]. Precipitation is not too adequate in the post-monsoon period to support the irrigation that requires either groundwater or surface water as a source.

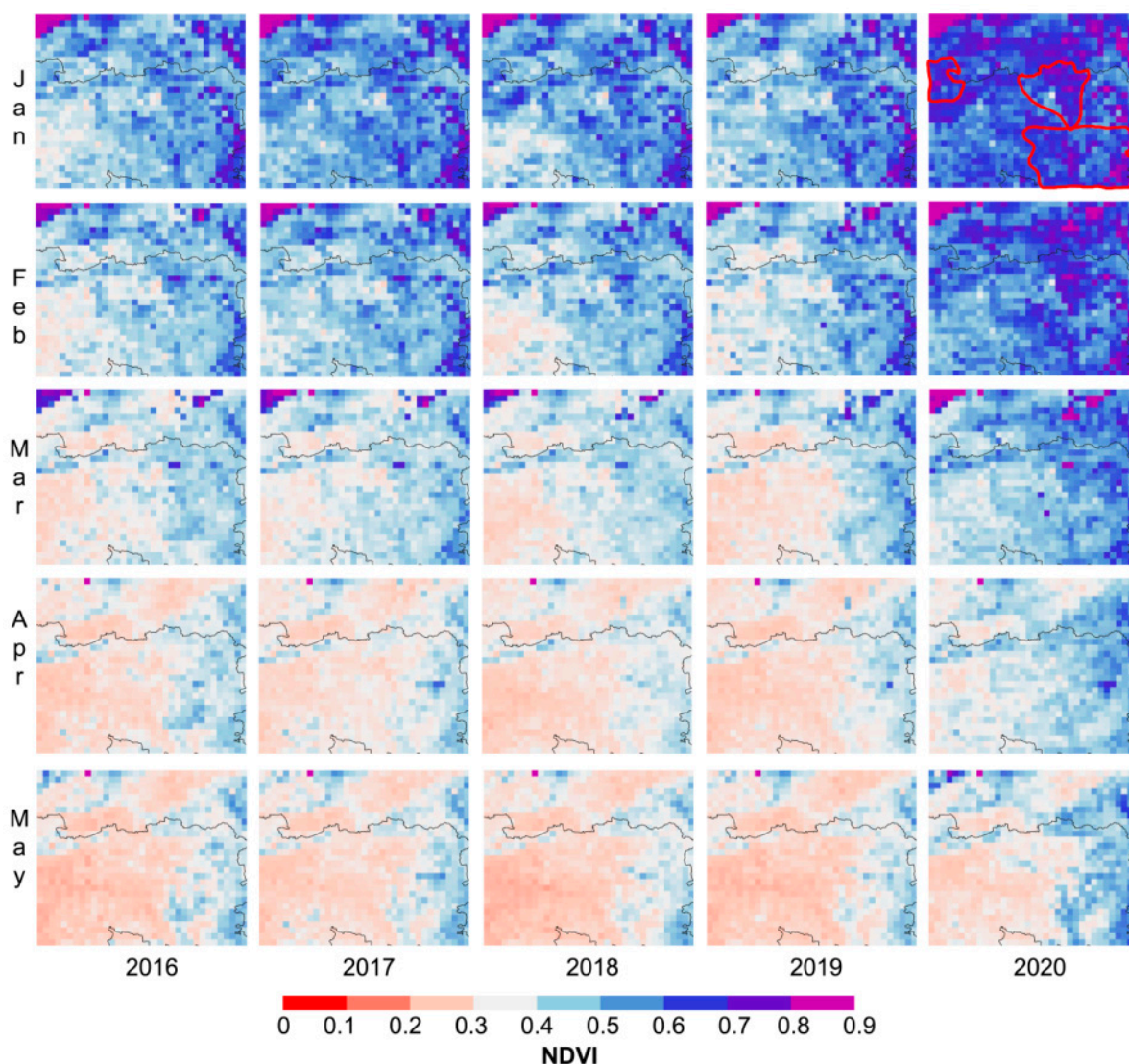


Figure 8. Normalized Difference Vegetation Index (NDVI) values in the study area during January to May in 2016–2020.

Monsoon precipitation patterns are highly variable and sudden shifts result in meteorological drought in Vidarbha. The region was subjected to 12 meteorological drought-years (annual precipitation rate was 26% or lesser than normal) from 1871 to 1984 [73]. The region

experienced 5–15% moderate meteorological drought-years in 1901–2003 [74]. Standardized precipitation index (SPI) based study indicates that the probability of occurrence of extreme drought is as high as 9% in 5 out of 16 districts within the study area [75]. The absence of major rivers and streams, as well as crystalline rock covered subsurface structure, requires water managers to adopt rain water harvesting in the study region to ensure water availability in non-monsoonal months. Water management policy implementation in the form of constructing tanks and other surface water structures also facilitates groundwater recharge and reduces water loss through evapotranspiration. These might play a key role in the TWSA replenishment observed in recent years. The typical structure of the monsoon is 4 months of precipitation with >90% of annual precipitation coverage, leaving the pre-monsoon (April–May) time dry with minimal TWSA. However, the COVID-19 lockdown imposed the lowering of irrigational activities, which might have played an important role in improving TWSA during April–May of 2020, with positive TWSA values that were estimated comparing all monthly TWSA including monsoonal months during April 2002 and May 2020. On a final note, the reduced human activity-linked rise in TWSA in April–May 2020 exhibits an improved water storage situation that represents a ‘once in a century’ scenario in such a drought prone area, where millions of dollars have already been spent toward this cause [4,32,58–60]. The lockdown-linked curb of pumping is also a rare phenomenon that encourages studies on groundwater storage change. Future studies could look at estimating groundwater recharge without, or minimally influenced by, irrigation.

5. Conclusions

We investigated the short- and long-term patterns in TWSA in the water scarce regions of central India, where a massive number of farmer suicides are taking place. Major findings of our study include an overall rise in the TWSA trend observed in recent years. Precipitation patterns cannot explain the rising TWSA trend, while the implementation of multiple sustainable water management policies might be the reason. Observation of positive TWSA during April–May 2020 might be associated with the reduction in human activities, including irrigation, due to the imposed lockdown to control the spread of COVID-19. On comparing the NDVI data in January to May between 2016 and 2020, along with crop data, higher NDVI values in 2020 were attributed to the rise in cotton production in four districts of Maharashtra state. TWSA forecasting using multiple statistical approaches indicate a rise in TWSA at the rates of 3.65 to 19.32 km³ in the area during May 2020, most likely linked to COVID-19 lockdown imposed reductions in irrigational activities.

Supplementary Materials: The following supporting information can be downloaded at: <https://www.mdpi.com/article/10.3390/rs14081768/s1>, Figure S1: Annual mean (April to March) precipitation in the study region.

Author Contributions: Conceptualization, S.N.B.; methodology, S.N.B.; software, S.N.B.; validation, S.N.B.; formal analysis, S.N.B.; investigation, S.N.B.; resources, S.N.B.; data curation, S.N.B.; writing—original draft preparation, S.N.B.; writing—review and editing, S.N.B. and M.S.; visualization, S.N.B. All authors have read and agreed to the published version of the manuscript.

Funding: This research received no external funding.

Data Availability Statement: Authors acknowledge the following data sources that were used in this study. GRACE TWS change data source: https://grace.jpl.nasa.gov/data/get-data/jpl_global_masc ons/ last accessed on 25 July 2021. GLDAS ET data source: <https://disc.gsfc.nasa.gov/datasets?keywords=evapotranspiration&sort=-timeRes&page=1&source=Models%2FAnalyses%20OBSERVATION%20BASED> accessed on 25 July 2021. CHIRPS data source: <https://www.chc.ucsb.edu/data/chirps> accessed on 25 July 2021. Land use land cover data for 2005 was obtained from the Oak Ridge National Laboratory’s (ORNL) database: https://daac.ornl.gov/cgi-bin/dsvviewer.pl?ds_id=1336 accessed on 25 July 2021. Irrigation area data were obtained from the AQUASTAT database of the Food and Agricultural Organization (FAO) of the United Nations: <http://www.fao.org/aquastat/en/geospatial-information/global-maps-irrigated-areas/latest-version> accessed on 25 July 2021. NDVI data are obtained from the NASA Earthdata repository: <https://lpdaac.usgs.gov/tools/earthdata-search/>

accessed on 25 July 2021. Crop data are obtained from <http://krishi.maharashtra.gov.in/>, <http://mpkrishi.mp.gov.in/> and <http://aps.dac.gov.in/> accessed on 20 September 2021.

Acknowledgments: S.N.B. acknowledges the support from the Indian Institute of Science in the form of C. V. Raman Postdoctoral Fellowship for carrying out the study.

Conflicts of Interest: The authors declare no conflict of interest.

References

- Bhanja, S.N.; Mukherjee, A.; Saha, D.; Velicogna, I.; Famiglietti, J.S. Validation of GRACE based groundwater storage anomaly using in-situ groundwater level measurements in India. *J. Hydrol.* **2016**, *543*, 729–738. [CrossRef]
- Rao, S.A.; Chaudhari, H.S.; Pokhrel, S.; Goswami, B.N. Unusual central Indian drought of summer monsoon 2008: Role of southern tropical Indian Ocean warming. *J. Clim.* **2010**, *23*, 5163–5174. [CrossRef]
- Venkateswarlu, B.; Raju, B.M.K.; Rao, K.V.; Rao, C.R. Revisiting drought-prone districts in India. *Econ. Political Wkly.* **2014**, *49*, 71–75.
- Verma, S.; Shah, M. Drought-Proofing through Groundwater Recharge: Lessons from Chief Ministers' Initiatives in Four Indian States. World Bank Group. 2019. Available online: <http://documents1.worldbank.org/curated/en/281991579881831723/pdf/Drought-Proofing-through-Groundwater-Recharge-Lessons-from-Chief-Ministers-Initiatives-in-Four-Indian-States.pdf> (accessed on 19 September 2020).
- Behere, P.B.; Behere, A.P. Farmers' suicide in Vidarbha region of Maharashtra state: A myth or reality? *Indian J. Psychiatry* **2008**, *50*, 124. [CrossRef] [PubMed]
- Dongre, A.R.; Deshmukh, P.R. Farmers' suicides in the Vidarbha region of Maharashtra, India: A qualitative exploration of their causes. *J. Inj. Violence Res.* **2012**, *4*, 2. [CrossRef]
- National Crime Records Bureau (NCRB). Accidental Deaths & Suicides in India 2015, Table 2A.3. National Crime Records Bureau, Government of India. 2016. Available online: https://ncrb.gov.in/sites/default/files/adsi_reports_previous_year/table-2A.3.pdf (accessed on 15 September 2020).
- WHO. WHO Coronavirus (COVID-19) Dashboard. 2022. Available online: <https://covid19.who.int/table> (accessed on 25 February 2022).
- Ministry of Health and Family Welfare (MOHFW), 2022. COVID-19 Statewise Status. Ministry of Health and Family Welfare, Govt. of India. Available online: <https://www.mohfw.gov.in/> (accessed on 26 February 2022).
- Box, G.E.; Jenkins, G.M. *Time Series Analysis Forecasting and Control*; Wisconsin University Madison Department of Statistics, Holden-Day: Madison, WI, USA, 1970; p. 553.
- Hodgson, F.D. The use of multiple linear regression in simulating ground-water level responses. *Groundwater* **1978**, *16*, 249–253. [CrossRef]
- Salas, J.D. *Applied Modeling of Hydrologic Time Series*; Water Resources Publication: Washington, DC, USA, 1980.
- Yaseen, Z.M.; El-Shafie, A.; Jaafar, O.; Afan, H.A.; Sayl, K.N. Artificial intelligence based models for stream-flow forecasting: 2000–2015. *J. Hydrol.* **2015**, *530*, 829–844. [CrossRef]
- Jain, S.K.; Das, A.; Srivastava, D.K. Application of ANN for reservoir inflow prediction and operation. *J. Water Resour. Plan. Manag.* **1999**, *125*, 263–271. [CrossRef]
- Daliakopoulos, I.N.; Coulibaly, P.; Tsanis, I.K. Groundwater level forecasting using artificial neural networks. *J. Hydrol.* **2005**, *309*, 229–240. [CrossRef]
- Shen, C.; Laloy, E.; Elshorbagy, A.; Albert, A.; Bales, J.; Chang, F.J.; Ganguly, S.; Hsu, K.L.; Kifer, D.; Fang, Z.; et al. HESS Opinions: Incubating deep-learning-powered hydrologic science advances as a community. *Hydrol. Earth Syst. Sci.* **2018**, *22*, 5639–5656. [CrossRef]
- Malakar, P.; Mukherjee, A.; Bhanja, S.N.; Sarkar, S.; Saha, D.; Ray, R.K. Deep learning-based forecasting of groundwater level trends in India: Implications for crop production and drinking water supply. *ACS ES&T Eng.* **2021**, *1*, 965–977.
- Nearing, G.S.; Kratzert, F.; Sampson, A.K.; Pelissier, C.S.; Klotz, D.; Frame, J.M.; Prieto, C.; Gupta, H.V. What role does hydrological science play in the age of machine learning? *Water Resour. Res.* **2021**, *57*, e2020WR028091. [CrossRef]
- Tapley, B.D.; Bettadpur, S.; Ries, J.C.; Thompson, P.F.; Watkins, M.M. GRACE measurements of mass variability in the Earth system. *Science* **2004**, *305*, 503–505. [CrossRef] [PubMed]
- Famiglietti, J.S.; Rodell, M. Water in the balance. *Science* **2013**, *340*, 1300–1301. [CrossRef]
- Rodell, M.; Famiglietti, J.S.; Wiese, D.N.; Reager, J.T.; Beaudoin, H.K.; Landerer, F.W.; Lo, M.H. Emerging trends in global freshwater availability. *Nature* **2018**, *557*, 651–659. [CrossRef]
- Wahr, J.M. Time-variable gravity from satellites. *Treatise Geophys.* **2007**, *3*, 213–237.
- Flechtner, F. *AOD1B Product Description Document for Product Releases 1 to 4 (Rev. 3.1, 13 April 2007)*; GRACE Project Document; GeoForschungszentrum: Potsdam, Germany, 2007; p. 43.
- Roy, P.S.; Meiyappan, P.K.; Joshi, M.P.; Kale, V.K.; Srivastava, S.K.; Srivastava, M.D.; Behera, A.; Roy, Y.; Sharma, R.M.; Ramachandran, P.; et al. *Decadal Land Use and Land Cover Classifications across India, 1985, 1995, 2005*; ORNL DAAC: Oak Ridge, TN, USA, 2016. [CrossRef]

25. Siebert, S.; Henrich, V.; Frenken, K.; Burke, J. *Global Map of Irrigation Areas Version 5*; Rheinische Friedrich-Wilhelms-University: Bonn, Germany; Food, Agriculture Organization of the United Nations: Rome, Italy, 2013; Volume 2, pp. 1299–1327.
26. Central Ground Water Board (CGWB). *Aquifer Systems of India*; G.o.I. Ministry of Water Resources: New Delhi, India, 2012; 92p.
27. Saha, D.; Marwaha, S.; Mukherjee, A. Groundwater resources and sustainable management issues in India. In *Clean and Sustainable Groundwater in India*; Springer: Singapore, 2018; pp. 1–11.
28. Bhanja, S.N.; Mukherjee, A.; Rodell, M.; Wada, Y.; Chattopadhyay, S.; Velicogna, I.; Pangaluru, K.; Famiglietti, J.S. Groundwater rejuvenation in parts of India influenced by water-policy change implementation. *Sci. Rep.* **2017**, *7*, 7453. [[CrossRef](#)]
29. Watkins, M.M.; Wiese, D.N.; Yuan, D.-N.; Boening, C.; Landerer, F.W. Improved methods for observing Earth's time variable mass distribution with GRACE using spherical cap mascons. *J. Geophys. Res. Solid Earth* **2015**, *120*, 2648–2671. [[CrossRef](#)]
30. Wiese, D.N.; Landerer, F.W.; Watkins, M.M. Quantifying and reducing leakage errors in the JPL RL05M GRACE mascon solution. *Water Resour. Res.* **2016**, *52*, 7490–7502. [[CrossRef](#)]
31. Wiese, N.D.; Yuan, D.-N.; Boening, C.; Landerer, F.W.; Watkins, M.M. JPL GRACE Mascon Ocean, Ice, and Hydrology Equivalent Water Height Release 06 Coastal Resolution Improvement (CRI) Filtered Version 1.0. PO. DAAC, CA, USA. 2018. Available online: https://podaac.jpl.nasa.gov/dataset/TELLUS_GRACE_MASCON_CRI_GRID_RL06_V1 (accessed on 25 July 2020). [[CrossRef](#)]
32. Patel, P.M.; Saha, D.; Shah, T. Sustainability of groundwater through community-driven distributed recharge: An analysis of arguments for water scarce regions of semi-arid India. *J. Hydrol. Reg. Stud.* **2020**, *29*, 100680. [[CrossRef](#)]
33. Cheng, M.; Tapley, B.D. Variations in the Earth's oblateness during the past 28 years. *J. Geophys. Res.* **2004**, *109*, B09402. [[CrossRef](#)]
34. Geruo, A.; Wahr, J.; Zhong, S. Computations of the viscoelastic response of a 3-D compressible Earth to surface loading: An application to Glacial Isostatic Adjustment in Antarctica and Canada. *Geophys. J. Int.* **2013**, *192*, 557–572. [[CrossRef](#)]
35. Funk, C.; Peterson, P.; Landsfeld, M.; Pedreros, D.; Verdin, J.; Shukla, S.; Husak, G.; Rowland, J.; Harrison, L.; Hoell, A.; et al. The climate hazards infrared precipitation with stations—A new environmental record for monitoring extremes. *Sci. Data* **2015**, *2*, 150066. [[CrossRef](#)]
36. Prakash, S. Performance assessment of CHIRPS, MSWEP, SM2RAIN-CCI, and TMPA precipitation products across India. *J. Hydrol.* **2019**, *571*, 50–59. [[CrossRef](#)]
37. Yoon, Y.; Kumar, S.V.; Forman, B.A.; Zaitchik, B.F.; Kwon, Y.; Qian, Y.; Rupper, S.; Maggioni, V.; Houser, P.; Kirschbaum, D.; et al. Evaluating the uncertainty of terrestrial water budget components over High Mountain Asia. *Front. Earth Sci.* **2019**, *7*, 120. [[CrossRef](#)]
38. Rodell, M.; Houser, P.R.; Jambor, U.E.A.; Gottschalck, J.; Mitchell, K.; Meng, C.J.; Arsenault, K.; Cosgrove, B.; Radakovich, J.; Bosilovich, M.; et al. The global land data assimilation system. *Bull. Am. Meteorol. Soc.* **2004**, *85*, 381–394. [[CrossRef](#)]
39. Li, X.; Long, D.; Han, Z.; Scanlon, B.R.; Sun, Z.; Han, P.; Hou, A. Evapotranspiration estimation for Tibetan plateau headwaters using conjoint terrestrial and atmospheric water balances and multisource remote sensing. *Water Resour. Res.* **2019**, *55*, 8608–8630. [[CrossRef](#)]
40. Ma, N.; Szilagyi, J. The CR of evaporation: A calibration-free diagnostic and benchmarking tool for large-scale terrestrial evapotranspiration modeling. *Water Resour. Res.* **2019**, *55*, 7246–7274. [[CrossRef](#)]
41. Pascolini-Campbell, M.A.; Reager, J.T.; Fisher, J.B. GRACE-based mass conservation as a validation target for basin-scale evapotranspiration in the contiguous United States. *Water Resour. Res.* **2020**, *56*, e2019WR026594. [[CrossRef](#)]
42. Contreras, J.; Espinola, R.; Nogales, F.J.; Conejo, A.J. ARIMA models to predict next-day electricity prices. *IEEE Trans. Power Syst.* **2003**, *18*, 1014–1020. [[CrossRef](#)]
43. Zhang, G.P. Time series forecasting using a hybrid ARIMA and neural network model. *Neurocomputing* **2003**, *50*, 159–175. [[CrossRef](#)]
44. Hyndman, R.J.; Athanasopoulos, G. *Forecasting: Principles and Practice*; OTexts: Heathmont, Australia, 2018.
45. Brown, R.G. *Statistical Forecasting for Inventory Control*; McGraw/Hill: New York, NY, USA, 1959.
46. Holt, C.C. *Planning Production, Inventories, and Work Force*; Prentice-Hall: Englewood Cliff, NJ, USA, 1960; Chapter 14.
47. Brown, R.G. *Smoothing, Forecasting and Prediction of Discrete Time Series*; Prentice-Hall: Englewood Cliff, NJ, USA, 1963.
48. Gardner, E.S., Jr. Exponential smoothing: The state of the art. *J. Forecast.* **1985**, *4*, 1–28. [[CrossRef](#)]
49. Gardner, E.S., Jr. Exponential smoothing: The state of the art—Part II. *Int. J. Forecast.* **2006**, *22*, 637–666. [[CrossRef](#)]
50. Cleveland, R.B.; Cleveland, W.S.; McRae, J.E.; Terpenning, I. STL: A seasonal-trend decomposition. *J. Off. Stat.* **1990**, *6*, 3–73.
51. De Livera, A.M.; Hyndman, R.J.; Snyder, R.D. Forecasting time series with complex seasonal patterns using exponential smoothing. *J. Am. Stat. Assoc.* **2011**, *106*, 1513–1527. [[CrossRef](#)]
52. Moriasi, D.N.; Arnold, J.G.; van Liew, M.W.; Bingner, R.L.; Harmel, R.D.; Veith, T.L. Model evaluation guidelines for systematic quantification of accuracy in watershed simulations. *Trans. ASABE* **2007**, *50*, 885–900. [[CrossRef](#)]
53. Nash, J.E.; Sutcliffe, J.V. River flow forecasting through conceptual models part I—A discussion of principles. *J. Hydrol.* **1970**, *10*, 282–290. [[CrossRef](#)]
54. Gupta, H.V.; Sorooshian, S.; Yapo, P.O. Status of automatic calibration for hydrologic models: Comparison with multilevel expert calibration. *J. Hydrol. Eng.* **1999**, *4*, 135–143. [[CrossRef](#)]
55. Helsel, D.R.; Hirsch, R.M. *Statistical Methods in Water Resources*; Elsevier: Amsterdam, The Netherlands, 1992; p. 49.
56. Hodrick, R.J.; Prescott, E.C. Postwar US business cycles: An empirical investigation. *J. Money Credit. Bank* **1997**, *29*, 1–16. [[CrossRef](#)]

57. Ravn, M.O.; Uhlig, H. On adjusting the Hodrick-Prescott filter for the frequency of observations. *Rev. Econ. Stat.* **2002**, *84*, 371–376. [[CrossRef](#)]
58. Department of Agriculture and Cooperation (DAC). *Vidarbha Intensive Irrigation Development Programme (VIIDP)*; Ministry of Agriculture, Government of India: New Delhi, India, 2012; p. 8. Available online: <http://agricoop.nic.in/sites/default/files/VIIDP.pdf> (accessed on 10 September 2020).
59. Law and Judiciary Department (LJD). *The Maharashtra Management of Irrigation Systems by Farmers act 2005*; Law and Judiciary Department, Government of Maharashtra: Mumbai, Maharashtra. Available online: <https://lj.maharashtra.gov.in/Site/Upload/Acts/5-The%20Maha.Mment%20of%20Irri.Sys.byFarmer%20Act-2005.pdf> (accessed on 19 September 2020).
60. World Bank. *Maharashtra Project on Climate Resilient Agriculture*; World Bank Group: Washington, DC, USA, 2018; Available online: <https://documents.worldbank.org/en/publication/documents-reports/documentdetail/704731519959668277/india-maharashtra-project-on-climate-resilient-agriculture-project> (accessed on 25 September 2020).
61. Central Water Commission (CWC). *National Register of Large Dams–2018*; Central Water Commission: New Delhi, India, 2018; p. 224. Available online: <http://cwc.gov.in/national-register-large-dams> (accessed on 23 September 2020).
62. Central Ground Water Board (CGWB). *Master Plan for Artificial Recharge to Ground Water in India*; G.o.I. Ministry of Water Resources: New Delhi, India, 2013; 225p.
63. Bhusari, V.; Katpatal, Y.B.; Kundal, P. An innovative artificial recharge system to enhance groundwater storage in basaltic terrain: Example from Maharashtra, India. *Hydrogeol. J.* **2016**, *24*, 1273–1286. [[CrossRef](#)]
64. Frappart, F.; Ramillien, G.; Ronchail, J. Changes in terrestrial water storage versus rainfall and discharges in the Amazon basin. *Int. J. Climatol.* **2013**, *33*, 3029–3046. [[CrossRef](#)]
65. Prakash, S.; Gairola, R.M.; Papa, F.; Mitra, A.K. An assessment of terrestrial water storage, rainfall and river discharge over Northern India from satellite data. *Curr. Sci.* **2014**, *107*, 1582–1586.
66. Didan, K. MOD13C2 MODIS/Terra Vegetation Indices Monthly L3 Global 0.05Deg CMG V006 [Data Set]. NASA EOSDIS Land Processes DAAC. 2015. Available online: <https://doi.org/10.5067/MODIS/MOD13C2.006> (accessed on 25 July 2020).
67. United States Geological Survey (USGS). NDVI, the Foundation for Remote Sensing Phenology. 2020. Available online: https://www.usgs.gov/core-science-systems/eros/phenology/science/ndvi-foundation-remote-sensing-phenology?qt-science_center_objects=0#qt-science_center_objects (accessed on 22 September 2020).
68. Bhanja, S.N.; Malakar, P.; Mukherjee, A.; Rodell, M.; Mitra, P.; Sarkar, S. Using satellite-based vegetation cover as indicator of groundwater storage in natural vegetation areas. *Geophys. Res. Lett.* **2019**, *46*, 8082–8092. [[CrossRef](#)]
69. Vittal, K.P.R.; Sinha, P.K.; Chary, G.R.; Sankar, G.M.; Srijaya, T.; Ramakrishna, Y.S.; Samra, J.S.; Singh, G. Districtwise promising technologies for rainfed rice based production system in India. In *All India Co-ordinated Research Project for Dryland Agriculture*; Central Research Institute for Dryland Agriculture, Indian Council of Agricultural Research: Hyderabad, India, 2004; Volume 500, p. 59.
70. Dalezios, N.R.; Domenikiotis, C.; Loukas, A.; Tzortzios, S.T.; Kalaitzidis, C. Cotton yield estimation based on NOAA/AVHRR produced NDVI. *Phys. Chem. Earth Part B Hydrol. Ocean. Atmos.* **2001**, *26*, 247–251. [[CrossRef](#)]
71. Tan, C.W.; Zhang, P.P.; Zhou, X.X.; Wang, Z.X.; Xu, Z.Q.; Mao, W.; Li, W.X.; Huo, Z.Y.; Guo, W.S.; Yun, F. Quantitative monitoring of leaf area index in wheat of different plant types by integrating NDVI and Beer-Lambert law. *Sci. Rep.* **2020**, *10*, 929. [[CrossRef](#)]
72. Agropedia. Cultivation of Wheat. *Indian Institute of Technology Kanpur*. 2020. Available online: <http://agropedia.iitk.ac.in/content/cultivation-wheat> (accessed on 21 September 2020).
73. Parthasarathy, B.; Sontakke, N.A.; Monot, A.A.; Kothawale, D.R. Droughts/floods in the summer monsoon season over different meteorological subdivisions of India for the period 1871–1984. *J. Climatol.* **1987**, *7*, 57–70. [[CrossRef](#)]
74. Pai, D.S.; Sridhar, L.; Guhathakurta, P.; Hatwar, H.R. District-wide drought climatology of the southwest monsoon season over India based on standardized precipitation index (SPI). *Nat. Hazards* **2011**, *59*, 1797–1813. [[CrossRef](#)]
75. Guhathakurta, P.; Menon, P.; Inkane, P.M.; Krishnan, U.; Sable, S.T. Trends and variability of meteorological drought over the districts of India using standardized precipitation index. *J. Earth Syst. Sci.* **2017**, *126*, 120. [[CrossRef](#)]